Research article

Zhicheng Xiao and Andrea Alù*

Tailoring exceptional points in a hybrid PT-symmetric and anti-PT-symmetric scattering system

https://doi.org/10.1515/nanoph-2021-0245
Received May 17, 2021; accepted July 9, 2021;
published online July 26, 2021

Abstract: Fano resonances feature an asymmetric lineshape with controllable linewidth, stemming from the interplay between bright and dark resonances. They provide efficient opportunities to shape the scattering lineshape, but they usually lack flexibility and tunability and are hindered by loss in passive systems. Here, we explore a hybrid parity-time (PT) and anti-parity-time (APT) symmetric system supporting unitary scattering features with highly tunable Fano resonances. The PT-APT-symmetric system can be envisioned in nanophotonic and microwave circuit implementations, allowing for real-time control of the scattering lineshape and its underlying singularities. Our study shows the opportunities enabled by non-Hermitian platforms to control scattering lineshapes for a plethora of photonic, electronic, and quantum systems, with potential for high-resolution imaging, switching, sensing, and multiplexing.

Keywords: circuits; nanophotonics; non-Hermitian; PT symmetry.

1 Introduction

Prof. Mark Stockman has pioneered research in enhanced light–matter interactions based on nanophotonic phenomena [1–4], demonstrating superb opportunities for extreme light confinement and manipulation relying on passive and active nanostructures. A common fingerprint of extreme wave-matter interactions in nanostructures is the Fano resonance [5–9], characterized by an asymmetric lineshape supported by the interaction between a bright, usually broad, resonance and discrete dark resonant states. This feature, emerging in a broad range of different photonic and electromagnetic platforms, has been utilized to develop several exciting applications, ranging from ultrafast optical switching [10], observation of molecule-level chemical dynamics [11], and nonlinearity-induced nonreciprocity [12]. These responses are typically imprinted within the complex nanostructure geometry, with challenges in reconfigurability. Being able to dynamically control and tune the Fano response in real-time would open new opportunities in a variety of contexts and applications. A few approaches have been proposed to this end, such as attosecond laser control [13, 14], geometrical phase control [15], and electrical control [16]. However, these approaches rely on complicated experimental setups, suffer from material loss, and are fundamentally limited in the range of transformations of Fano resonances that may be available and in terms of real-time control and tuning range.

In a parallel effort, active nanophotonic systems have been recently gaining significant attention in the optics community, again following the pioneering work of Prof. Stockman on nanolasing and spasers [1, 17–19]. Recent efforts in this area have been exploring in particular systems with balanced loss and gain elements, which support exotic scattering features, including unidirectional invisibility [17–23], single-mode lasing [24, 25], robust information transfer [26], enhanced sensing [27, 28], among several other applications [29–33]. Balanced loss and gain distributions in space support a Hamiltonian H^{PT} that is invariant under a dual parity and time-reversal operation: $[\mathrm{PT}, H^{\mathrm{PT}}] = 0$, which is known as parity-time (PT) symmetry [34–44]. A variant, known as anti-parity-time (APT) symmetry, is defined as $H^{\mathrm{APT}} = \pm iH^{\mathrm{PT}}$, which has also led to the recent discovery of various intriguing phenomena [45–54].

***Corresponding author**: **Andrea Alù**, Department of Electrical and Computer Engineering, The University of Texas at Austin, Austin, TX 78712, USA; Photonics Initiative, Advanced Science Research Center, City University of New York, New York, NY 10031, USA; and Physics Program, Graduate Center, City University of New York, New York, NY 10016, USA, E-mail: aalu@gc.cuny.edu. https://orcid.org/0000-0002-4297-5274
Zhicheng Xiao, Department of Electrical and Computer Engineering, The University of Texas at Austin, Austin, TX 78712, USA. https://orcid.org/0000-0002-9027-3058

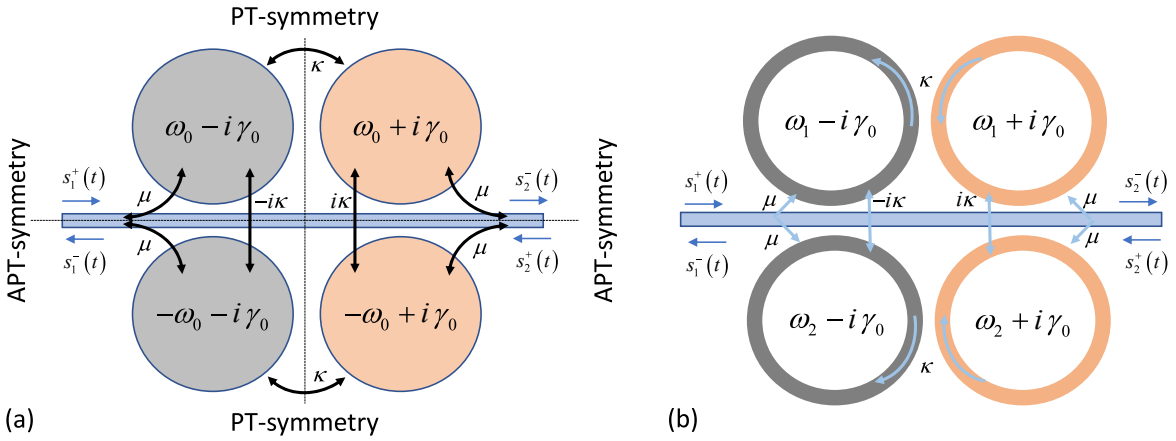

Figure 1: (a) Conceptual schematic of a hybrid PT-APT-symmetric system. The system is PT-symmetric with respect to the vertical axis and APT-symmetric with respect to the horizontal axis. Coupling between the resonator and the waveguide is μ and coupling between resonators is κ on the vertical axis and $\pm i\kappa$ on the horizontal axis, where κ is purely real and μ is a complex parameter function of the scattering matrix of the direct process. $\pm\omega_0$ are the resonant frequencies and $\pm\gamma_0$ are the gain/loss parameter. (b) A nanophotonic implementation based on four active/passive ring resonators and a bus waveguide.

In this work, we study a hybrid PT-APT-symmetric geometry with two orthogonal axes of symmetry, showcasing unique scattering features and opportunities to realize efficient control of the spectral response. The proposed system consists of four coupled loss/gain nanoresonators, PT-symmetric along the vertical axis and APT-symmetric along the horizontal axis (see Figure 1). By coupling this system to a two-port waveguide, we demonstrate that it supports a unitary scattering process ($S^\dagger S = \mathbf{I}$), where S is the scattering matrix and $\mathbf{I}$ is a unity matrix having the same dimension as S, † is the conjugate transpose operator. The scattering system demonstrates a wide control over the location of its scattering singularities, reflected in widely tunable resonance spectra by controlling its design parameters. The points at which the spectrum dramatically changes in lineshape correspond to exceptional points (EPs) [44] of the isolated Hamiltonian of the PT-APT-symmetric system, which are defined as the symmetry phase transition points of the eigenfrequencies. Based on these features, the proposed system allows for real-time control of Fano resonances by tuning the coupling parameter, offering interesting opportunities for sensing and dynamic filters.

2 Hybrid PT-APT-symmetric system

The PT-APT-symmetric system is schematically shown in Figure 1a, and possible nanophotonic implementation in the form of four nanoring resonators coupled to a bus waveguide is shown in Figure 1b. Looking at the system around the vertical axis, it is formed by two pairs of PT-symmetric resonators with resonances $\pm\omega_0$, gain/loss rates $\pm\gamma_0$, and coupling coefficient κ. Across the horizontal axis, the same system can be described as two pairs of APT-symmetric resonators: one is a pair of gain resonators with lossy coupling coefficient $i\kappa$, the other is a pair of lossy resonators with gain coupling coefficient $-i\kappa$. Therefore, the Hamiltonian of this system reads as

$$H = \begin{bmatrix} \omega_0 + i\gamma_0 & \kappa & 0 & i\kappa \\ \kappa & \omega_0 - i\gamma_0 & -i\kappa & 0 \\ 0 & -i\kappa & -\omega_0 - i\gamma_0 & \kappa \\ i\kappa & 0 & \kappa & -\omega_0 + i\gamma_0 \end{bmatrix}. \quad (1)$$

Although our system obeys both PT-symmetry and APT-symmetry, the PT operator does not commute with H or $\pm iH$, which means $[\mathrm{PT}, H] \neq 0$ and $[\mathrm{PT}, \pm iH] \neq 0$. The system can be categorized as a general non-Hermitian system, which has peculiar degeneracies and exotic scattering features if coupled to a waveguide due to its non-diagonalizable Hamiltonian around the supported EPs.

To facilitate the exploration of the scattering features, we study its eigenfrequency spectrum. By simplifying the associated characteristic equation $\mathrm{Det}|H - \mathbf{I}\omega| = 0$, we find

$$(\omega^2 - \omega_0^2 + \gamma_0^2)^2 + 4(\omega_0^2\gamma_0^2 - \omega_0^2\kappa^2 - \gamma_0^2\kappa^2) = 0, \quad (2)$$

where $\mathbf{I}$ is a unity matrix with the same dimension as the Hamiltonian. Figure 2 shows the real and imaginary parts of the eigenfrequencies, as a function of the coupling

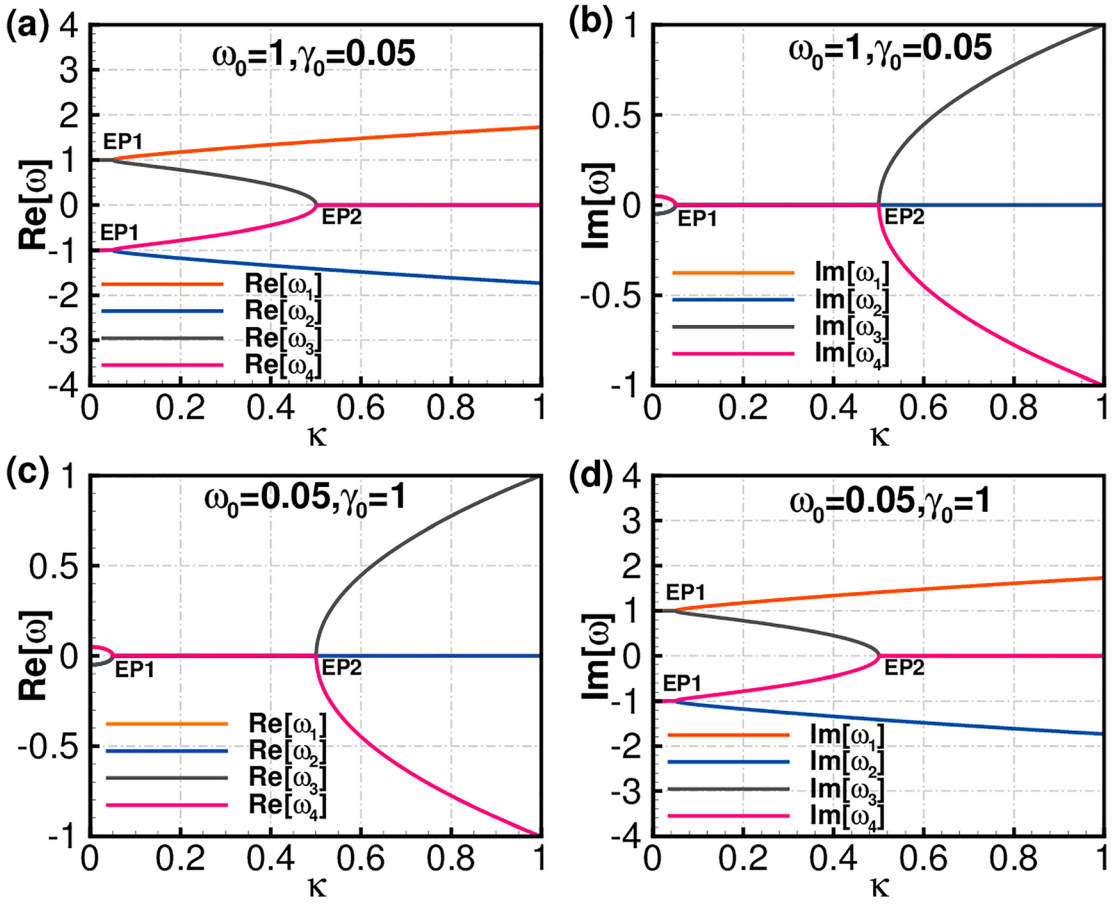

Figure 2: Eigenfrequencies and exceptional points.
(a) The real part of the eigenfrequencies for $\omega_0 = 1, \gamma_0 = 0.05$, we find two second-order EP when $\kappa = \frac{\omega_0\gamma_0}{\sqrt{\omega_0^2+\gamma_0^2}}$ and one second-order EP when $\kappa = \frac{\sqrt{\omega_0^2+\gamma_0^2}}{2}$. (b) The imaginary part of the eigenfrequencies for $\omega_0 = 1, \gamma_0 = 0.05$, we find a second-order EP when $\kappa = \frac{\omega_0\gamma_0}{\sqrt{\omega_0^2+\gamma_0^2}}$ and a second-order EP when $\kappa = \frac{\sqrt{\omega_0^2+\gamma_0^2}}{2}$. (c) The real part of the eigenfrequencies for $\omega_0 = 0.05, \gamma_0 = 1$, we find a second-order EP when $\kappa = \frac{\omega_0\gamma_0}{\sqrt{\omega_0^2+\gamma_0^2}}$ and one second-order EP when $\kappa = \frac{\sqrt{\omega_0^2+\gamma_0^2}}{2}$. (d) The imaginary part of the eigenfrequencies for $\omega_0 = 0.05, \gamma_0 = 1$, we find two second-order EPs for $\kappa = \frac{\omega_0\gamma_0}{\sqrt{\omega_0^2+\gamma_0^2}}$ and a second-order EP for $\kappa = \frac{\sqrt{\omega_0^2+\gamma_0^2}}{2}$.

coefficient κ, assuming a constant gain or loss rate γ_0 and resonance ω_0. The system supports a number of EPs along the real and imaginary frequency axes, which stem from the degeneracy of the Hamiltonian with a dimension larger than 2. The location of these EPs and corresponding degenerate eigenfrequencies are

$$\begin{aligned} \kappa_{EP1} &= \frac{\omega_0\gamma_0}{\sqrt{\omega_0^2+\gamma_0^2}}, \omega_{EP1} = \pm\sqrt{\omega_0^2-\gamma_0^2}; \\ \kappa_{EP2} &= \frac{\sqrt{\omega_0^2+\gamma_0^2}}{2}, \omega_{EP2} = \pm\sqrt{2(\omega_0^2-\gamma_0^2)}. \end{aligned} \tag{3}$$

It is easy to show that κ_{EP1} is always smaller or equal to κ_{EP2}, where $\kappa_{EP1} = \kappa_{EP2}$ if $\omega_0 = \gamma_0$. The latter case corresponds to a system with a fourth-order EP at $\kappa_{EP} = \omega_0/\sqrt{2}$ and $\omega_{EP} = 0$, which is a higher-order degeneracy point. Equations (2) and (3) also highlight a duality between ω_0 and γ_0 in this system, implying that the real and imaginary parts of the eigenfrequencies interchange with each other if we swap ω_0 and γ_0, as shown in Figure 2. Figure 2a and b plot the real and imaginary parts of the eigenfrequencies for $\omega_0 = 1, \gamma_0 = 0.05$. Swapping the values of ω_0 and γ_0, we interchange real and imaginary parts of the eigenfrequency spectrum, as shown in Figure 2c and d.

The case $\omega_0 > \gamma_0$ is naturally more relevant for nanophotonic applications. When the coupling coefficient κ is smaller than the value of the first EP, the four resonators act as almost mutually isolated, leading to unitary real eigenfrequencies and negligible imaginary eigenfrequencies. As the coupling grows and is tuned between

κ_{EP1} and κ_{EP2}, gain and loss in the resonators and coupling channels are balanced, implying that the system is in the exact PT-APT symmetry phase. We find purely real eigenfrequencies in this case. For coupling beyond the second EP, the eigenfrequencies are again complex, and the response enters a broken phase with growing and decaying modes. We show in the next section how we can control and tune the scattering features by manipulating the location of the EPs when the system is coupled to a bus waveguide.

3 Highly tunable Fano resonant response

Exotic scattering features emerge when our system is interrogated by a probing network, which may be represented by a coupled waveguide or incident radiation in the case of a scattering system. As shown in Figure 1b, we feed the four-ring resonators with a bus waveguide aligned with the horizontal axis to excite the system and retrieve its scattering features. The coupling coefficient between each resonator and the waveguide is defined by the complex quantity μ. Assuming that this system is excited with signals $s_1^+(t)$ and $s_2^+(t)$ on the left and right sides of the waveguide, respectively, the output signals are defined as $s_1^-(t)$ and $s_2^-(t)$. Coupled mode theory is a powerful tool to describe the mutual interaction between the system and the coupling waveguide, which in our case reads as [55–57]

$$\begin{cases} \dfrac{\mathrm{d}\mathbf{a}(t)}{\mathrm{d}t} = (-iH - \Gamma)\mathbf{a}(t) + K^{\mathrm{T}}\mathbf{s}^+(t), \\ \mathbf{s}^-(t) = C\mathbf{s}^+(t) + K\mathbf{a}(t), \end{cases} \tag{4}$$

where $\mathbf{a}(t) = \begin{bmatrix} a_1(t) & a_2(t) & a_3(t) & a_4(t) \end{bmatrix}^{\mathrm{T}}$ is the field amplitude inside the resonator, T is the transpose operator, $K = \mu\begin{bmatrix} 1 & 1 & 1 & 1 \\ 1 & 1 & 1 & 1 \end{bmatrix}$ is the coupling matrix, $\Gamma = K^{\dagger}K/2$ is the decaying loss matrix, † is a conjugate transpose operator, $C = \begin{bmatrix} r & t \\ t & r \end{bmatrix}$ is the direct scattering matrix when the coupled resonators are totally disconnected from the waveguide, r is the reflection coefficient, t is the transmission coefficient, and the lossless nature of the waveguide implies $C^{\dagger}C = \mathbf{I}$. $s^{\pm}(t) = \begin{bmatrix} s_1^{\pm}(t) & s_2^{\pm}(t) \end{bmatrix}^{\mathrm{T}}$ are the excitation and response state vectors, respectively.

By performing a Fourier transform of Eq. (4) and using the relation $CK^* = -K$ dictated by time-reversal symmetry [56, 57], we obtain the scattering matrix

$$S = C + iK(\omega\mathbf{I} - H + i\Gamma)^{-1}K^{\mathrm{T}}, \tag{5}$$

which is defined by the relation $\mathbf{s}^- = S\mathbf{s}^+$. Substituting the Hamiltonian from Eq. (1) into this equation, we obtain the detailed expressions:

$$\begin{aligned} S_{11} = S_{22} &= r - \frac{4i(r+t)\gamma_e\left[\omega^3 + \kappa\omega^2 + (\gamma_0^2 - 2\gamma_0\kappa - \omega_0^2)\omega + \gamma_0^2\kappa - 2\gamma_0\kappa^2 + \kappa\omega_0^2\right]}{\left(\omega^2 - \omega_0^2 + \gamma_0^2\right)^2 + 4\left(\gamma_0^2\omega_0^2 - \omega_0^2\kappa^2 - \gamma_0^2\kappa^2\right) + 4i\gamma_e\left[\omega^3 + \kappa\omega^2 + (\gamma_0^2 - 2\gamma_0\kappa - \omega_0^2)\omega + \gamma_0^2\kappa - 2\gamma_0\kappa^2 + \kappa\omega_0^2\right]} \\ S_{21} = S_{12} &= t - \frac{4i(r+t)\gamma_e\left[\omega^3 + \kappa\omega^2 + (\gamma_0^2 - 2\gamma_0\kappa - \omega_0^2)\omega + \gamma_0^2\kappa - 2\gamma_0\kappa^2 + \kappa\omega_0^2\right]}{\left(\omega^2 - \omega_0^2 + \gamma_0^2\right)^2 + 4\left(\gamma_0^2\omega_0^2 - \omega_0^2\kappa^2 - \gamma_0^2\kappa^2\right) + 4i\gamma_e\left[\omega^3 + \kappa\omega^2 + (\gamma_0^2 - 2\gamma_0\kappa - \omega_0^2)\omega + \gamma_0^2\kappa - 2\gamma_0\kappa^2 + \kappa\omega_0^2\right]} \end{aligned} \tag{6}$$

where γ_e is the decay rate from the resonator to the waveguide.

From this result, we find that $S^{\dagger}S = \mathbf{I}$, implying that our scattering system operates as a purely lossless system at any frequency, even in the broken phase regime in which the Hamiltonian of the isolated system supports complex eigenvalues. This result can be understood from two different perspectives: the system can be modeled as two PT-symmetric resonators side coupled to a waveguide. We show in Appendix A that a scattering system where a PT-symmetric resonator is side-coupled to a lossless waveguide acts as a lossless/gainless system. Hence, two side-coupled PT-symmetric systems are also expected to introduce no net gain or loss into the waveguide under this excitation scheme. On the other hand, the system can also be modeled as two complementary APT-symmetric systems. One of the APT-symmetric resonator pairs absorbs energy from the waveguide, as $S^{\dagger}S - \mathbf{I} < 0$ [Appendix B]; while the other APT-symmetric resonator pair pumps energy into the waveguide as $S^{\dagger}S - \mathbf{I} > 0$ [Appendix C]. The overall effect is that the scattering system remains neutral, despite the presence of gain and loss. The overall passivity of our scattering system can also be further confirmed by

studying the eigenvalues and eigenstates of the scattering matrix. We generally find two eigenvalues $\lambda_1 = r - t$ and $\lambda_2 = (r + t)e^{-2i\phi}$, and two corresponding eigenstates $|\Phi_\pm\rangle$, where ϕ is the phase of the denominator common to all scattering coefficients $S_{mn}, m = 1, 2, n = 1, 2$. The lossless condition of the direct scattering matrix $C^\dagger C = \mathbf{I}$ implies that $|\lambda_1| = |\lambda_2| = 1$, meaning that the system does not extract or impart energy to impinging waves for the arbitrary linear combination of scattering eigenstates.

The real part of the denominator in Eq. (6) corresponds to the characteristic Eq. (2), supporting interesting scattering features. When the excitation frequency is identical to an eigenfrequency, the scattering matrix becomes $S = \begin{bmatrix} -t & -r \\ -r & -t \end{bmatrix}$. If we assume that the waveguide is transparent, $r = 0, t = 1$, then the system at these frequencies fully reflects because of the resonant response, similar to the functionality of a bandstop filter. The scattering lineshape as a function of frequency can be engineered by setting the system in different regimes varying the coupling κ. When $\kappa \leq \kappa_{EP1}$, there is only one real eigenfrequency equal to ω_0. As shown in Figure 3a, the system, in this case, exhibits an asymmetric Fano resonance around ω_0, with very sharp features. When the coupling coefficient $\kappa_{EP1} \leq \kappa \leq \kappa_{EP2}$, we find two eigenfrequencies and, as shown in Figure 3b, the system exhibits an asymmetric Fano resonance around the first eigenfrequency and a symmetric Lorentzian resonance at the second one. When the coupling coefficient $\kappa \geq \kappa_{EP2}$, we find only one eigenfrequency, as in Figure 3c, and the system exhibits a symmetric Lorentzian resonance around such frequency. In all examples, it is evident that the system operates as a lossless passive filter, but with a large degree of manipulation of its spectrum as a function of the EP location enabled by its underlying non-Hermiticity. Our

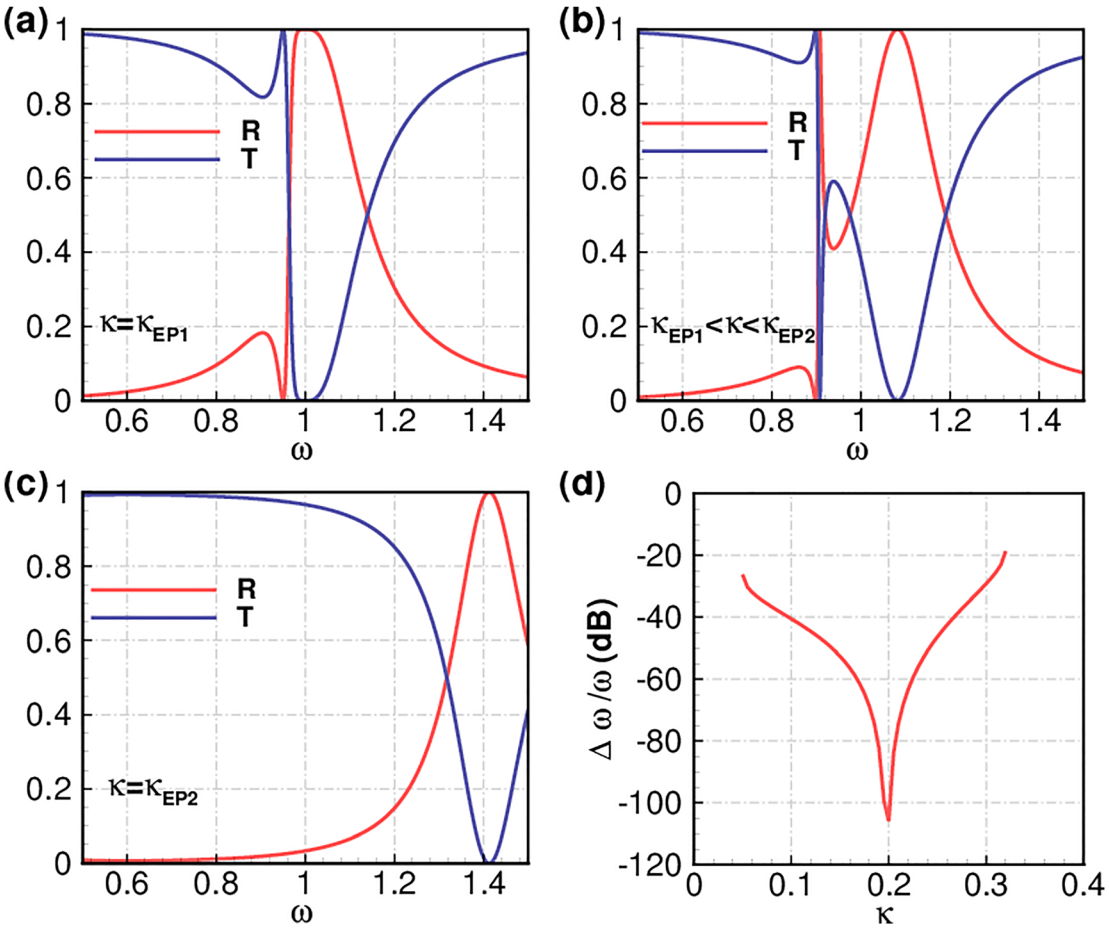

Figure 3: Drastic tailoring of the scattering spectrum with EP engineering in the PT-APT-symmetric system. *R* indicates reflectance and *T* transmittance.
(a) Fano power transmission and reflection lineshape as the system operates at the first EP: $\kappa = \kappa_{EP1}$. (b) Combined Fano and Lorentzian resonances when the system works between the first and second EP: $\kappa_{EP1} < \kappa < \kappa_{EP2}$. (c) Lorentzian transmission and reflection spectra when the system is at the second EP: $\kappa = \kappa_{EP2}$. (d) The fractional linewidth of the Fano resonance for $\kappa_{EP1} < \kappa < \kappa_{EP2}$. The following parameters are used: $\omega_0 = 1, \gamma_0 = 0.05, \gamma_e = 0.05, r = 0, t = 1$.

hybrid PT-APT-symmetric system can be engineered to control reflection and transmission lineshapes with interesting flexibility, changing smoothly from a Lorentzian to a Fano lineshape with arbitrary linewidth as the coupling parameter is varied. In particular, for systems in the exact PT-APT-symmetric phase, we find a sharp transition of the reflectance (or transmittance) from 0 to 1. In Figure 3d we show the fractional linewidth variations as a function of κ, showing a highly desirable response for sensing and switching applications.

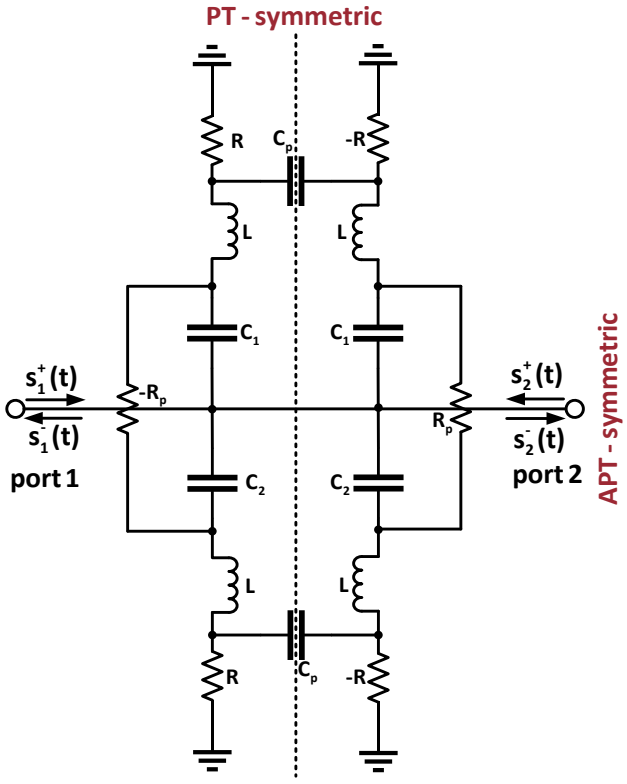

Figure 4: Realistic layout of a PT-APT-symmetric circuit. A pair of PT-symmetric LC resonators with inductance L, capacitance C_1, and positive (negative) resistance R ($-R$) are coupled by a capacitance C_p. Another pair of PT-symmetric LC resonators with inductance L, capacitance C_2, and positive (negative) resistance R ($-R$) are coupled by a capacitance C_p. The lossy resonator LC_1 and the lossy resonator LC_2 are coupled through a gain channel $-R_p$. The gain resonator LC_1 and the gain resonator LC_2 are coupled through a lossy channel R_p. The whole system is PT-symmetric along the vertical axis and APT-symmetric along the horizontal axis. The circuit parameters are: $L = 100\,\mu H$, $C_1 = 100\,pF$, $C_2 = 80\,pF$, $Z_0 = 50\,\Omega$, $R = 20\,\Omega$.

4 PT-APT-symmetric implementation in a microwave circuit

In this section, we explore the design of a PT-APT-symmetric system in a microwave circuit platform [58, 59], paving the way for real-time reconfigurability with variable capacitors. Similar designs may be pursued in nanophotonic implementations. Figure 4 shows a realistic implementation using lumped circuit elements. The loss and gain elements are represented by positive and negative resistance elements R and –R, in which for simplicity here we neglect the frequency dispersion of the active elements. The positive and negative resonance are realized by two series LC resonators with different resonant frequencies, $\omega_1 = 1/\sqrt{LC_1}$ and $\omega_2 = 1/\sqrt{LC_2}$. Positive and negative resistance R_p and $-R_p$ model the lossy and gain coupling channel; while C_p models the neutral coupling channel. The system in Figure 4 satisfies the required PT-APT symmetry [58, 59]. We show the corresponding scattering features in Figure 5 calculated with full-wave simulations. When $R_p = 100\,k\Omega$, $C_p = 1500\,pF$, the system is in the weak coupling regime and exhibits a sharp Fano resonance; when $R_p = 50\,k\Omega$, $C_p = 3000\,pF$, the system supports combined Fano and Lorentzian resonances; when $R_p = 5\,k\Omega$, $C_p = 50000\,pF$, the system is in the strong

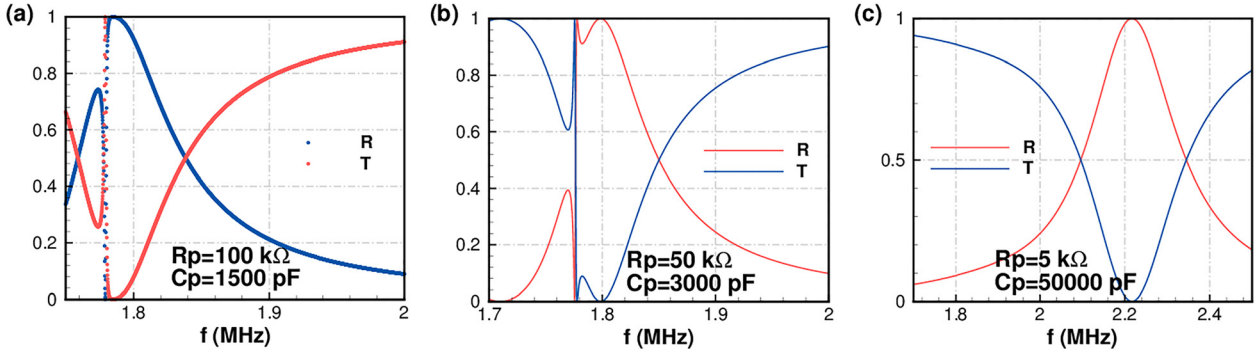

Figure 5: (a) Fano resonance in the weak coupling regime. (b) Fano and Lorentzian resonance in the intermediate coupling regime. (c) Lorentzian resonance in the strong coupling regime. Dashed lines in the subplot (a) comes from the abrupt change of the spectrum.

coupling regime and is now tuned to a broad Lorentzian resonance without sharp spectral features. This drastic evolution of the scattering spectra is associated with the tuning of the corresponding EPs of the system, similarly to the discussion in the previous section, which may be achieved by tuning the applied voltage to variable capacitors in the coupling channels.

5 Conclusions

In this work, we have explored a hybrid PT/APT-symmetric system unveiling the possibility of drastically controlling the scattering signature by manipulating the supported EPs varying the coupling parameter. This manipulation enables a dynamic and real-time tunability of reflection and transmission spectra between Fano and Lorentzian lineshape. We envision that these interesting scattering features can be practically realized in various open and guided nanophotonic settings opening prospects for imaging, filtering, sensing, and multiplexing applications, and showcasing the opportunities enabled by non-Hermitian systems and dispersion engineering in nanophotonics and electromagnetics, as pioneered throughout his scientific career by Prof. Mark Stockman. In particular, for nanophotonic settings these features may be enabled in coupled nanowaveguides loaded by gain and loss elements, or in coupled nanoparticles excited in the far-field, enabling highly unusual scattering phenomena.

Author contribution: All the authors have accepted responsibility for the entire content of this submitted manuscript and approved submission.
Research funding: This work is supported by the Office of Naval Research with grant No. N00014-19-1-2011 and the Simons Foundation.
Conflict of interest statement: The authors declare no conflicts of interest regarding this article.

Appendix A: PT-symmetric system side-coupled to a waveguide

Figure 6 demonstrates a PT-symmetric resonator pair side-coupled to a waveguide, in which the Hamiltonian is defined as

$$H = \begin{bmatrix} \omega_0 - i\gamma_0 & \kappa \\ \kappa & \omega_0 + i\gamma_0 \end{bmatrix}, \tag{A1}$$

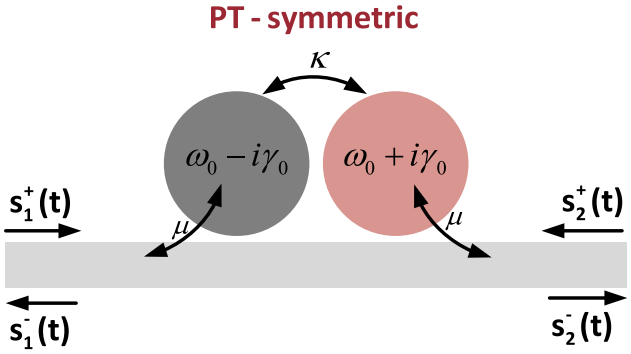

Figure 6: PT-symmetric system side-coupled to a waveguide.

where ω_0 is the resonant frequency, γ_0 is the intrinsic loss and gain rate in the first and second resonator, and κ is the coupling coefficient between the two resonators. The system is side-coupled to a waveguide with a coupling coefficient μ. For the above scattering system, the coupled mode equation is

$$\begin{cases} \dfrac{\mathrm{d}}{\mathrm{d}t}\begin{bmatrix} a_1 \\ a_2 \end{bmatrix} = (-iH - \Gamma)\begin{bmatrix} a_1 \\ a_2 \end{bmatrix} + K^T\begin{bmatrix} s_1^+ \\ s_2^+ \end{bmatrix}, \\ \begin{bmatrix} s_1^- \\ s_2^- \end{bmatrix} = \begin{bmatrix} r & t \\ t & r \end{bmatrix}\begin{bmatrix} s_1^+ \\ s_2^+ \end{bmatrix} + K\begin{bmatrix} a_1 \\ a_2 \end{bmatrix}, \end{cases} \tag{A2}$$

where $C = \begin{bmatrix} r & t \\ t & r \end{bmatrix}$ is the direct pathway scattering matrix and obeys unitary conditions $C^\dagger C = \mathbf{I}$, implying that $|r|^2 + |t|^2 = 1, rt^* + r^*t = 0$. $K = \mu\begin{bmatrix} 1 & 1 \\ 1 & 1 \end{bmatrix}$ is the coupling matrix between the waveguide and the cavity. According to the energy conservation law: $K^\dagger K = 2\Gamma$, we have $\Gamma = |\mu|^2\begin{bmatrix} 1 & 1 \\ 1 & 1 \end{bmatrix}, \gamma_e = |\mu|^2$, where γ_e is the decaying rate from the cavity to the waveguide.

Therefore, we have the following scattering parameters:

$$\begin{cases} S_{11} = S_{22} = r - \dfrac{i2(r+t)\gamma_e(\omega - \omega_0 + \kappa)}{(\omega - \omega_0)^2 + \gamma_0^2 - \kappa^2 + 2i\gamma_e(\omega - \omega_0 + \kappa)}, \\ S_{21} = S_{12} = t - \dfrac{i2(r+t)\gamma_e(\omega - \omega_0 + \kappa)}{(\omega - \omega_0)^2 + \gamma_0^2 - \kappa^2 + 2i\gamma_e(\omega - \omega_0 + \kappa)}. \end{cases} \tag{A3}$$

We can easily confirm that the scattering matrix satisfies the passivity condition $S^\dagger S = \mathbf{I}$ at any frequency. This means that the scattering system behaves as a purely lossless system. The scattering spectra for various coupling strengths are shown in Figure 7, confirming that the response is always consistent with a lossless system, and unveiling Fano and combined Fano and Lorentzian spectra.

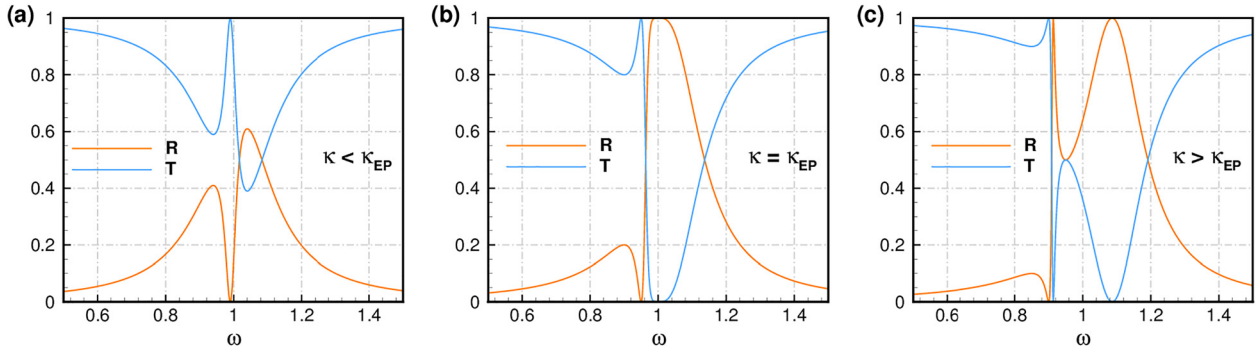

Figure 7: Power reflection and transmission spectra for $\omega_0 = 1, \gamma_0 = 0.05, \gamma_e = 0.05, r = 0, t = 1, \kappa_{EP} = 0.05$.
(a) Fano resonance with $\kappa < \kappa_{EP}$. (b) Fano resonance with $\kappa = \kappa_{EP}$. (c) Fano resonance plus Lorentzian resonance with $\kappa > \kappa_{EP}$.

Appendix B: APT-symmetric system with lossy resonators side-coupled to a waveguide

Figure 8 shows an APT-symmetric system side-coupled to a waveguide, in which the Hamiltonian is defined as

$$H = \begin{bmatrix} \omega_0 - i\gamma_0 & -i\kappa \\ -i\kappa & -\omega_0 - i\gamma_0 \end{bmatrix}, \tag{B1}$$

where ω_0 is the resonant frequency, γ_0 is the intrinsic loss rate in the first and second resonator, and $-i\kappa$ is the coupling coefficient between the two resonators. The system is side-coupled to a waveguide with a coupling coefficient μ. For the above scattering system, the coupled mode equation is

$$\begin{cases} \dfrac{\mathrm{d}}{\mathrm{d}t}\begin{bmatrix} a_1 \\ a_2 \end{bmatrix} = (-iH - \Gamma)\begin{bmatrix} a_1 \\ a_2 \end{bmatrix} + \mathrm{K}^{\mathrm{T}}\begin{bmatrix} s_1^+ \\ s_2^+ \end{bmatrix}, \\ \begin{bmatrix} s_1^- \\ s_2^- \end{bmatrix} = \begin{bmatrix} r & t \\ t & r \end{bmatrix}\begin{bmatrix} s_1^+ \\ s_2^+ \end{bmatrix} + \mathrm{K}\begin{bmatrix} a_1 \\ a_2 \end{bmatrix}, \end{cases} \tag{B2}$$

where $C = \begin{bmatrix} r & t \\ t & r \end{bmatrix}$ is the direct pathway scattering matrix and obeys unitary condition $C^\dagger C = \mathbf{I}$, implying that $|r|^2 + |t|^2 = 1, rt^* + r^* t = 0$. $K = \mu\begin{bmatrix} 1 & 1 \\ 1 & 1 \end{bmatrix}$ is the coupling matrix between the waveguide and the cavity. According to the energy conservation law: $K^\dagger K = 2\Gamma$, we have

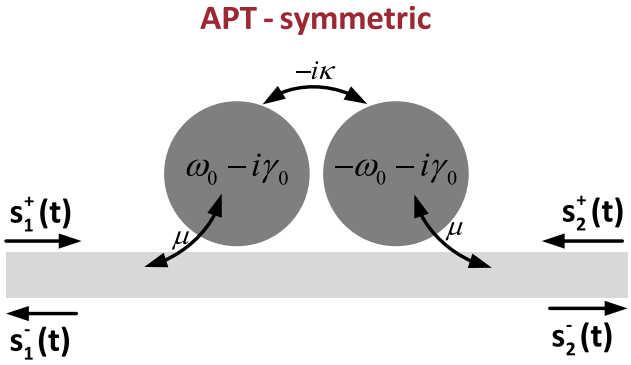

Figure 8: APT-symmetric system side-coupled to a waveguide.

$\Gamma = |\mu|^2\begin{bmatrix} 1 & 1 \\ 1 & 1 \end{bmatrix}, \gamma_e = |\mu|^2$, where γ_e is the decaying rate from the cavity to the waveguide.

Therefore, we have the following scattering parameters:

$$\begin{cases} S_{11} = S_{22} = r - \dfrac{i2(r+t)\gamma_e(\omega + i\gamma_0 - i\kappa)}{\omega^2 - \omega_0^2 - \gamma_0^2 + \kappa^2 + 2i\gamma_e(\omega + i\gamma_0 - i\kappa) + 2i\gamma_0\omega}, \\ S_{21} = S_{12} = t - \dfrac{i2(r+t)\gamma_e(\omega + i\gamma_0 - i\kappa)}{\omega^2 - \omega_0^2 - \gamma_0^2 + \kappa^2 + 2i\gamma_e(\omega + i\gamma_0 - i\kappa) + 2i\gamma_0\omega}. \end{cases} \tag{B3}$$

In the weak coupling regime $\kappa \ll \gamma_0 \ll \omega_0$, it is easy to show that

$$S^\dagger S - \mathbf{I} < 0, \tag{B4}$$

which implies that the APT-symmetric system absorbs energy from the waveguide. The reflection and transmission spectra are shown in Figure 9, which indicates that the APT-symmetric system only supports Lorentzian resonances.

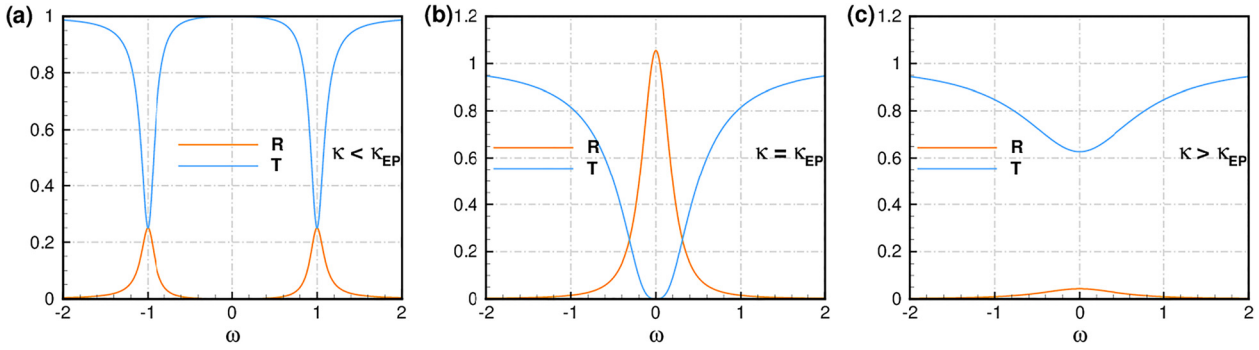

Figure 9: Power reflection and transmission spectrum for $\omega_0 = 1, \gamma_0 = 0.05, \gamma_e = 0.05, r = 0, t = 1$.
(a) Double Lorentzian resonances with $\kappa < \kappa_{EP}$. (b) Single Lorentzian resonance $\kappa = \kappa_{EP}$. (c) Single Lorentzian resonance with $\kappa > \kappa_{EP}$.

Appendix C: APT-symmetric system with gain resonator side-coupled to a waveguide

Figure 10 shows an APT-symmetric system side-coupled to a waveguide, in which the Hamiltonian is defined as

$$H = \begin{bmatrix} \omega_0 + i\gamma_0 & i\kappa \\ i\kappa & -\omega_0 + i\gamma_0 \end{bmatrix}, \tag{C1}$$

where ω_0 is the resonant frequency, γ_0 is the intrinsic gain rate in the first and second resonator, and $i\kappa$ is the coupling coefficient between the two resonators. The system is side-coupled to a waveguide with a coupling coefficient μ. For the above scattering system, the coupled mode equation is

$$\begin{cases} \dfrac{\mathrm{d}}{\mathrm{d}t}\begin{bmatrix} a_1 \\ a_2 \end{bmatrix} = (-iH - \Gamma)\begin{bmatrix} a_1 \\ a_2 \end{bmatrix} + \mathrm{K}^{\mathrm{T}}\begin{bmatrix} s_1^+ \\ s_2^+ \end{bmatrix}, \\ \begin{bmatrix} s_1^- \\ s_2^- \end{bmatrix} = \begin{bmatrix} r & t \\ t & r \end{bmatrix}\begin{bmatrix} s_1^+ \\ s_2^+ \end{bmatrix} + \mathrm{K}\begin{bmatrix} a_1 \\ a_2 \end{bmatrix}, \end{cases} \tag{C2}$$

where $C = \begin{bmatrix} r & t \\ t & r \end{bmatrix}$ is the direct pathway scattering matrix and obeys unitary conditions $C^\dagger C = \mathbf{I}$, implying that $|r|^2 + |t|^2 = 1, rt^* + r^* t = 0$. $K = \mu\begin{bmatrix} 1 & 1 \\ 1 & 1 \end{bmatrix}$ is the coupling matrix between the waveguide and the cavity. According to the energy conservation law: $K^\dagger K = 2\Gamma$, we have

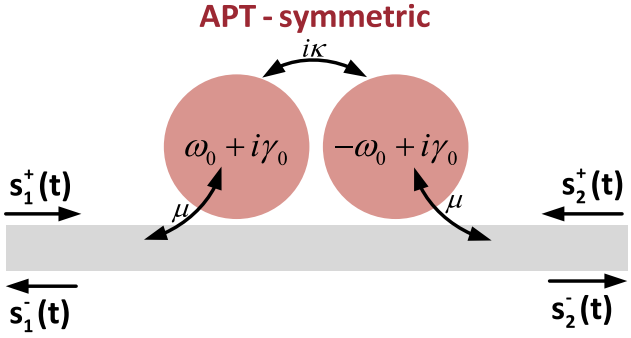

Figure 10: APT-symmetric system side-coupled to a waveguide.

$\Gamma = |\mu|^2\begin{bmatrix} 1 & 1 \\ 1 & 1 \end{bmatrix}, \gamma_e = |\mu|^2$, where γ_e is the decaying rate from the cavity to the waveguide.

Therefore, we have the following scattering parameters

$$\begin{cases} S_{11} = S_{22} = r - \dfrac{i2(r+t)\gamma_e(\omega - i\gamma_0 + i\kappa)}{\omega^2 - \omega_0^2 - \gamma_0^2 + \kappa^2 + 2i\gamma_e(\omega - i\gamma_0 + i\kappa) - 2i\gamma_0\omega}, \\ S_{21} = S_{12} = t - \dfrac{i2(r+t)\gamma_e(\omega - i\gamma_0 + i\kappa)}{\omega^2 - \omega_0^2 - \gamma_0^2 + \kappa^2 + 2i\gamma_e(\omega - i\gamma_0 + i\kappa) - 2i\gamma_0\omega}. \end{cases} \tag{C3}$$

In the weak coupling regime $\kappa \ll \gamma_0 \ll \omega_0$, it is easy to show that

$$S^\dagger S - \mathbf{I} > 0, \tag{C4}$$

which implies that the APT-symmetric system pumps energy into the waveguide. The reflection and transmission spectra are shown in Figure 11, which indicates that the APT-symmetric system with gain only supports Lorentzian resonances, and do not behave as a passive system.

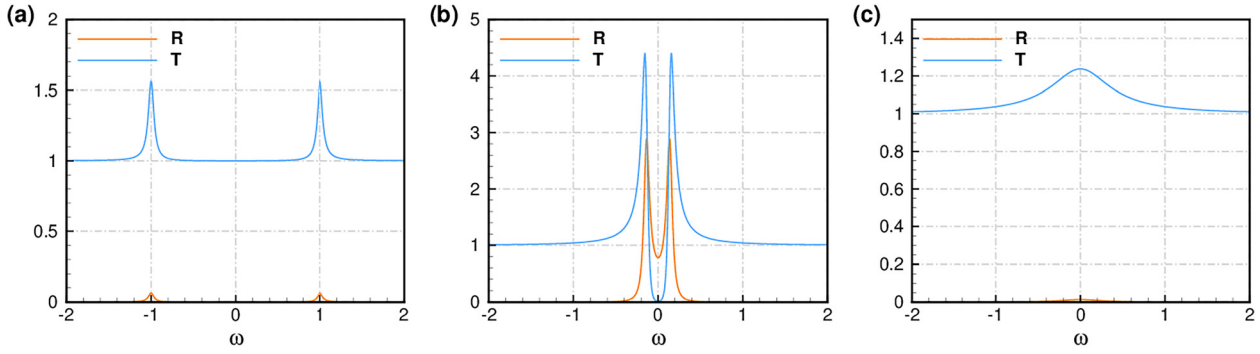

Figure 11: Power reflection and transmission spectra for $\omega_0 = 1, \gamma_0 = 0.05, \gamma_e = 0.01, r = 0, t = 1$.
(a) Double Lorentzian resonances with $\kappa < \kappa_{EP}$. (b) Single Lorentzian resonance $\kappa = \kappa_{EP}$. (c) Single Lorentzian resonance with $\kappa > \kappa_{EP}$.

References

[1] D. J. Bergman and M. I. Stockman, "Surface plasmon amplification by stimulated emission of radiation: quantum generation of coherent surface plasmons in nanosystems," *Phys. Rev. Lett.*, vol. 90, 2003, Art no. 027402.

[2] M. I. Stockman, "Nanofocusing of optical energy in tapered plasmonic waveguides," *Phys. Rev. Lett.*, vol. 93, 2004, Art no. 137404.

[3] M. I. Stockman, "The spaser as a nanoscale quantum generator and ultrafast amplifier," *J. Opt.*, vol. 12, 2010, Art no. 024004.

[4] M. I. Stockman, "Nanoplasmonics: past, present, and glimpse into future," *Opt. Express*, vol. 19, p. 22029, 2011.

[5] A. E. Miroshnichenko, S. Flach, and Y. S. Kivshar, "Fano resonances in nanoscale structures," *Rev. Mod. Phys.*, vol. 82, p. 2257, 2010.

[6] B. Luk'yanchuk, N. I. Zheludev, S. A. Maier, et al., "The Fano resonance in plasmonic nanostructures and metamaterials," *Nat. Mater.*, vol. 9, p. 707, 2010.

[7] M. F. Limonov, M. V. Rybin, A. N. Poddubny, and Y. S. Kivshar, "Fano resonances in photonics," *Nat. Photonics*, vol. 11, p. 543, 2017.

[8] E. H. Hasdeo, A. R. T. Nugraha, K. Sato, M. S. Dresselhaus, and R. Saito, "Electronic Raman scattering and the Fano resonance in metallic carbon nanotubes," *Phys. Rev. B*, vol. 88, 2013, Art no. 115107.

[9] Y. Zhang, Y.-R. Zhen, O. Neumann, J. K. Day, P. Nordlander, and N. J. Halas, "Coherent anti-Stokes Raman scattering with single-molecule sensitivity using a plasmonic Fano resonance," *Nat. Commun.*, vol. 5, p. 4424, 2014.

[10] L. Stern, M. Grajower, and U. Levy, "Fano resonances and all-optical switching in a resonantly coupled plasmonic-atomic system," *Nat. Commun.*, vol. 5, p. 4865, 2014.

[11] R. Y. Bello, S. E. Canton, D. Jelovina, et al., "Reconstruction of the time-dependent electronic wave packet arising from molecular autoionization," *Sci. Adv.*, vol. 4, p. 3962, 2018.

[12] D. L. Sounas, J. Soric, and A. Alù, "Broadband passive isolators based on coupled nonlinear resonances," *Nat. Electron.*, vol. 1, p. 113, 2018.

[13] C. Ott, A. Kaldun, P. Raith, et al., "Lorentz meets Fano in spectral line shapes: a universal phase and its laser control," *Science*, vol. 340, p. 716, 2013.

[14] A. Kaldun, A. Blättermann, V. Stooß, et al., "Observing the ultrafast buildup of a Fano resonance in the time domain," *Science*, vol. 354, p. 738, 2016.

[15] S. K. Ray, A. K. Singh, Ajmal, S. Chandel, P. Mitra, and N. Ghosh, *Controlling Fano Resonance Using the Geometrical Phase of Light in Spatially Tailored Waveguided Plasmonic Crystals*. arxiv.org/abs/1905.01636.

[16] Y. Vardi, E. Cohen-Hoshen, G. Shalem, and I. Bar-Joseph, "Fano Resonance in an electrically driven plasmonic device," *Nano Lett.*, vol. 16, p. 748, 2016.

[17] M. I. Stockman, "Spaser action, loss compensation, and stability in plasmonic systems with gain," *Phys. Rev. Lett.*, vol. 106, 2011, Art no. 156802.

[18] S. I. Azzam, A. V. Kildishev, R.-M. Ma, et al., "Ten years of spasers and plasmonic nanolasers," *Light Sci. Appl.*, vol. 9, p. 90, 2020.

[19] J.-S. Wu, V. Apalkov, and M. I. Stockman, "Topological spaser," *Phys. Rev. Lett.*, vol. 124, 2020, Art no. 017701.

[20] Z. Lin, H. Ramezani, T. Eichelkraut, T. Kottos, H. Cao, and D. N. Christodoulides, "Unidirectional invisibility induced by PT-symmetric periodic structures," *Phys. Rev. Lett.*, vol. 106, 2011, Art no. 213901.

[21] R. Fleury, D. Sounas, and A. Alù, "An invisible acoustic sensor based on parity-time symmetry," *Nat. Commun.*, vol. 6, p. 5905, 2015.

[22] D. L. Sounas, R. Fleury, and A. Alù, "Unidirectional cloaking based on metasurfaces with balanced loss and gain," *Phys. Rev. Appl.*, vol. 4, 2015, Art no. 014005.

[23] N. X. A. Rivolta and B. Maes, "Side-coupled resonators with parity-time symmetry for broadband unidirectional invisibility," *Phys. Rev. A*, vol. 94, 2016, Art no. 053854.

[24] H. Hodaei, M.-A. Miri, M. Heinrich, D. N. Christodoulides, and M. Khajavikhan, "Parity-time-symmetric microring lasers," *Science*, vol. 346, p. 975, 2014.

[25] L. Feng, Z. J. Wong, R.-M. Ma, Y. Wang, and X. Zhang, "Single-mode laser by parity-time symmetry breaking," *Science*, vol. 346, p. 972, 2014.

[26] Z. Xiao, Y. Radi, S. Tretyakov, and A. Alù, "Microwave tunneling and robust information transfer based on parity-time-symmetric absorber-emitter pairs," *Research*, vol. 2019, p. 10, 2019.

[27] P.-Y. Chen, M. Sakhdari, M. Hajizadegan, et al., "Generalized parity–time symmetry condition for enhanced sensor telemetry," *Nat. Electron.*, vol. 1, p. 297, 2018.

[28] Z. Xiao, H. Li, T. Kottos, and A. Alù, "Enhanced sensing and nondegraded thermal noise performance based on

PT-symmetric electronic circuits with a sixth-order exceptional point," *Phys. Rev. Lett.*, vol. 123, 2019, Art no. 213901.
[29] H. Alaeian and J. A. Dionne, "Parity-time-symmetric plasmonic metamaterials," *Phys. Rev. A*, vol. 89, 2014, Art no. 03382.
[30] W. Wang, L. Q. Wang, R. D. Xue, et al., "Unidirectional excitation of radiative-loss-free surface plasmon polaritons in PT-symmetric systems," *Phys. Rev. Lett.*, vol. 119, 2017, Art no. 077401.
[31] M. Sakhdari, M. Hajizadegan, Q. Zhong, D. N. Christodoulides, R. El-Ganainy, and P. Y. Chen, "Experimental observation of PT-symmetry breaking near divergent exceptional points," *Phys. Rev. Lett.*, vol. 123, 2019, Art no. 193901.
[32] M. Farhat, M. Yang, Z. Ye, and P. Y. Chen, "PT-symmetric absorber-laser enables electromagnetic sensors with unprecedented sensitivity," *ACS Photonics*, vol. 7, p. 2080, 2020.
[33] M. Sakhdari, N. Mohammadi Estakhri, H. Bagci, and P. Y. Chen, "Low-threshold lasing and coherent perfect absorption in generalized PT-symmetric optical structures," *Phys. Rev. Appl.*, vol. 10, 2018, Art no. 024030.
[34] C. M. Bender and S. Boettcher, "Real spectra in non-Hermitian Hamiltonians having PT symmetry," *Phys. Rev. Lett.*, vol. 80, p. 5243, 1998.
[35] C. M. Bender, "Making sense of non-Hermitian Hamiltonians," *Rep. Prog. Phys.*, vol. 70, p. 947, 2007.
[36] R. El-Ganainy, K. G. Makris, D. N. Christodoulides, and Z. H. Musslimani, "Theory of coupled optical PT-symmetric structures," *Opt. Lett.*, vol. 32, p. 2632, 2007.
[37] C. E. Rüter, K. G. Makris, R. El-Ganainy, D. N. Christodoulides, M. Segev, and D. Kip, "Observation of parity-time symmetry in optics," *Nat. Phys.*, vol. 6, p. 192, 2010.
[38] J. Schindler, A. Li, M. C. Zheng, F. M. Ellis, and T. Kottos, "Experimental study of active LRC circuits with PT symmetries," *Phys. Rev. A*, vol. 84, 2011, Art no. 040101.
[39] Z. Lin, J. Schindler, F. M. Ellis, and T. Kottos, "Experimental observation of the dual behavior of PT-symmetric scattering," *Phys. Rev. A*, vol. 85, 2012, Art no. 050101.
[40] J. Schindler, Z. Lin, J. M. Lee, H. Ramezani, F. M. Ellis, and T. Kottos, "PT-symmetric electronics," *J. Phys. A: Math. Theor.*, vol. 45, 2012, Art no. 444029.
[41] L. Ge, Y. D. Chong, and A. D. Stone, "Conservation relations and anisotropic transmission resonances in one-dimensional PT-symmetric photonic heterostructures," *Phys. Rev. A*, vol. 85, 2012, Art no. 023802.
[42] J. Li, R. Yu, C. Ding, and Y. Wu, "PT-symmetry-induced evolution of sharp asymmetric line shapes and high-sensitivity refractive index sensors in a three-cavity array," *Phys. Rev. A*, vol. 93, 2016, Art no. 023814.
[43] S. Tanaka, S. Garmon, K. Kanki, and T. Petrosky, "Higher-order time-symmetry-breaking phase transition due to meeting of an exceptional point and a Fano resonance," *Phys. Rev. A*, vol. 94, 2016, Art no. 022105.
[44] M.-A. Miri and A. Alù, "Exceptional points in optics and photonics," *Science*, vol. 63, p. 7709, 2019.
[45] P. Peng, W. Cao, C. Shen, et al., "Anti-parity-time symmetry with flying atoms," *Nat. Phys.*, vol. 12, p. 1139, 2016.
[46] F. Yang, Y.-C. Liu, and L. You, "Anti-PT symmetry in dissipatively coupled optical systems," *Phys. Rev. A*, vol. 96, 2017, Art no. 053845.
[47] L. Jin, "Scattering properties of a parity-time-antisymmetric non-Hermitian system," *Phys. Rev. A*, vol. 98, 2018, Art no. 022117.
[48] Y. Choi, C. Hahn, J. W. Yoon, and S. H. Song, "Observation of an anti-PT-symmetric exceptional point and energy-difference conserving dynamics in electrical circuit resonators," *Nat. Commun.*, vol. 9, p. 2182, 2018.
[49] V. V. Konotop and D. A. Zezyulin, "Odd-time reversal PT symmetry induced by an Anti PT-symmetric medium," *Phys. Rev. Lett.*, vol. 120, 2018, Art no. 123902.
[50] Y. Li, Y.-G. Peng, L. Han, et al., "Anti-parity-time symmetry in diffusive systems," *Science*, vol. 364, p. 170, 2019.
[51] Q. Li, C.-J. Zhang, Z.-D. Cheng, et al., "Experimental simulation of anti-parity-time symmetric Lorentz dynamics," *Optica*, vol. 6, p. 67, 2019.
[52] T. Shui, W.-X. Yang, L. Li, and X. Wang, "Lop-sided Raman-Nath diffraction in PT-antisymmetric atomic lattices," *Opt. Lett.*, vol. 44, p. 2089, 2019.
[53] Z. Ye, M. Farhat, and P.-Y. Chen, "Tunability and switching of Fano and Lorentz resonances in PTX-symmetric electronic systems," *App. Phys. Lett.*, vol. 117, 2020, Art no. 031101.
[54] A. Bergman, R. Duggan, K. Sharma, M. Tur, A. Zadok, and A. Alù, "Observation of anti-parity-time-symmetry, phase transitions and exceptional points in an optical fiber," *Nat. Commun.*, vol. 12, p. 486, 2021.
[55] S. Fan, "Sharp asymmetric line shapes in side-coupled waveguide-cavity systems," *Appl. Phys. Lett.*, vol. 80, p. 908, 2002.
[56] S. Fan, W. Suh, and J. D. Joannopoulos, "Temporal coupled-mode theory for the Fano resonance in optical resonators," *J. Opt. Soc. Am. A*, vol. 20, p. 569, 2003.
[57] S. Wonjoo, W. Zheng, and F. Shanhui, "Temporal coupled-mode theory and the presence of non-orthogonal modes in lossless multimode cavities," *IEEE J. Quant. Electron.*, vol. 40, p. 1511, 2004.
[58] B. Lv, R. Li, J. Fu, et al., "Analysis and modeling of Fano resonances using equivalent circuit elements," *Sci. Rep.*, vol. 6, p. 31884, 2016.
[59] D. M. Pozar, *Microwave Engineering*, 4th ed., New York, Wiley, 2011.